INTERNATIONAL JOURNAL FOR NUMERICAL METHODS IN FLUIDS, VOL. 11, 719–749 (1990)

COMPRESSIBLE VISCOUS FLOW CALCULATIONS USING COMPATIBLE FINITE ELEMENT APPROXIMATIONS

M. O. BRISTEAU
INRIA, BP 105, F-78153 Le Chesnay Cedex, France

R. GLOWINSKI
University of Houston, Houston, TX 77004, U.S.A.

AND

L. DUTTO, J. PÉRIAUX AND G. ROGÉ
AMD/BA, BP 300, F-92214 St Cloud Cedex, France

SUMMARY

We discuss in this paper the numerical simulation of compressible viscous flows by a combination of finite element methods for the space approximation, an implicit second-order multistep scheme for the time discretization and GMRES iterative methods for solving the non-linear problems encountered at each time step. Numerical results corresponding to flows around aerofoils and aerospace vehicles illustrate the possibilities of these methods.

KEY WORDS Compressible Navier–Stokes FEM Non-linear solver Compatible approximations

1. INTRODUCTION

In Reference 1 we discussed the numerical solution of the compressible Navier–Stokes equations by operator-splitting methods. In this paper we consider the solution of the same problem by methods which are in a sense more implicit since they are based on a time discretization by an implicit second-order multistep scheme. This scheme is combined with finite element methods for the space discretization and with a GMRES algorithm with preconditioning to solve the non-linear problems encountered at each time step.

An important issue which is discussed here is the necessity (at least with the centred space approximations used here) to use different finite element approximations for velocity and density. The necessity for such a compatibility condition, which is well known in the incompressible case, has been discussed for a simple compressible case in Reference 2; from the numerical experiments of Section 6, this compatibility condition seems also to be required for more complicated compressible flows.

In addition to the experiments of Section 6, the methods discussed in this paper are used to simulate flows around aerofoils and (three-dimensional) aerospace vehicles.

0271–2091/90/140719–31$15.50

Received November 1989

2. THE COMPRESSIBLE NAVIER–STOKES EQUATIONS

Let $\Omega \subset R^N$ ($N = 2, 3$ in practice) be the flow domain and Γ be its boundary. The non-dimensional conservative form of the equations is given by

$$\frac{\partial \rho}{\partial t} + \nabla \cdot \rho \mathbf{u} = 0, \tag{1}$$

$$\frac{\partial \rho \mathbf{u}}{\partial t} + \nabla \cdot (\rho \mathbf{u} \otimes \mathbf{u}) + \nabla p = \frac{1}{Re}[\Delta \mathbf{u} + \tfrac{1}{3}\nabla(\nabla \cdot \mathbf{u})], \tag{2}$$

$$\frac{\partial e}{\partial t} + \nabla \cdot (e+p)\mathbf{u} = \frac{1}{Re}\left(\nabla \cdot [\mathbf{u}(-\tfrac{2}{3}\nabla \cdot \mathbf{u} + \nabla \mathbf{u} + \nabla \mathbf{u}^{\mathrm{T}})] + \frac{\gamma}{Pr}\Delta \varepsilon\right), \tag{3}$$

with ρ, $\mathbf{u}$ and T the density, velocity and temperature variables respectively.

The pressure obeys the ideal gas law

$$p = (\gamma - 1)\rho \varepsilon, \tag{4}$$

and for the total energy e we have

$$e = \rho \varepsilon + \rho |\mathbf{u}|^2/2. \tag{5}$$

The above equations express the conservation of mass, momentum and energy. We normalize the temperature T by $|\mathbf{u}_r|^2/c_v$, implying that

$$T = \varepsilon. \tag{6}$$

The constants Re, Pr and γ are the Reynolds number, the Prandtl number and the ratio of specific heats respectively ($\gamma = 1{\cdot}4$ in air).

From (1)–(6) we can deduce the following non-conservative form of the Navier–Stokes equations:

$$\frac{\partial \rho}{\partial t} + \mathbf{u} \cdot \nabla \rho + \rho \nabla \cdot \mathbf{u} = 0, \tag{7}$$

$$\frac{\partial \mathbf{u}}{\partial t} + (\mathbf{u} \cdot \nabla)\mathbf{u} + (\gamma - 1)\left(\frac{T}{\rho}\nabla \rho + \nabla T\right) = \frac{1}{Re\rho}[\Delta \mathbf{u} + \tfrac{1}{3}\nabla(\nabla \cdot \mathbf{u})], \tag{8}$$

$$\frac{\partial T}{\partial t} + \mathbf{u} \cdot \nabla T + (\gamma - 1)T \nabla \cdot \mathbf{u} = \frac{1}{Re\rho}\left(\frac{\gamma}{Pr}\Delta T + F(\nabla \mathbf{u})\right), \tag{9}$$

where (4)–(6) still hold.

For three-dimensional flows we have $\mathbf{u} = \{u, v, w\}$, and $F(.)$ in (9) has the following expression:

$$F(\nabla \mathbf{u}) = \frac{4}{3}\left[\left(\frac{\partial u}{\partial x}\right)^2 + \left(\frac{\partial v}{\partial y}\right)^2 + \left(\frac{\partial w}{\partial z}\right)^2\right] + \left(\frac{\partial v}{\partial x} + \frac{\partial u}{\partial y}\right)^2 + \left(\frac{\partial w}{\partial x} + \frac{\partial u}{\partial z}\right)^2 + \left(\frac{\partial v}{\partial z} + \frac{\partial w}{\partial y}\right)^2 - \frac{4}{3}\left(\frac{\partial u}{\partial x}\frac{\partial v}{\partial y} + \frac{\partial u}{\partial x}\frac{\partial w}{\partial z} + \frac{\partial v}{\partial y}\frac{\partial w}{\partial z}\right). \tag{10}$$

In this paper we will consider mainly the non-conservative form (7)–(10) of the equations written as a function of the primitive variables; in this case the expression of the different terms is much simpler.

Boundary and initial conditions have to be added.

We consider external flows; the domain of computation is described in Figure 1. Let Γ_∞ be the

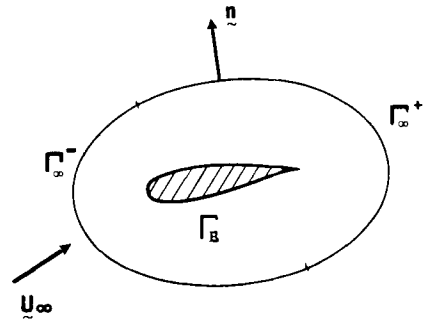

Figure 1. Computational domain

far-field boundary of the domain; we introduce then

$$\Gamma_\infty^- = \{x \mid x \in \Gamma_\infty, \mathbf{u}_\infty \cdot \mathbf{n} < 0\}, \tag{11}$$

$$\Gamma_\infty^+ = \Gamma_\infty \setminus \Gamma_\infty^-, \tag{12}$$

where $\mathbf{u}_\infty$ denotes the free-stream velocity and $\mathbf{n}$ the unit vector of the outward normal to Γ.

We assume the flow to be uniform at infinity and the corresponding variables to be normalized by the free-stream values. We require on the upstream boundary Γ_∞^- the following conditions:

$$\mathbf{u} = \mathbf{u}_\infty = \begin{pmatrix} \cos\alpha \\ \sin\alpha \end{pmatrix}, \tag{13}$$

$$\rho = 1, \tag{14}$$

$$T = T_\infty = 1/\gamma(\gamma-1)M_\infty^2, \tag{15}$$

where α is the angle of attack and M_∞ denotes the free-stream Mach number. On the downstream boundary Γ_∞^+ we require Neumann boundary conditions on $\mathbf{u}$ and T, i.e.

$$\partial \mathbf{u}/\partial n = 0, \tag{16}$$

$$\partial T/\partial n = 0, \tag{17}$$

and if $M_\infty < 1$ we prescribe also on Γ_∞^+

$$\rho = 1. \tag{18}$$

On the rigid boundary Γ_B we shall use the following conditions:

$$\mathbf{u} = 0 \quad \text{(no-slip condition)}, \tag{19}$$

$$T = T_B = T_\infty[1 + (\gamma-1)M_\infty^2/2] \quad \text{(free-stream total temperature)}. \tag{20}$$

Finally, since we consider time-dependent equations (even if we are looking for steady solutions), initial conditions have to be added; we shall take

$$\rho(x, 0) = \rho_0(x), \tag{21}$$

$$\mathbf{u}(x, 0) = \mathbf{u}_0(x), \tag{22}$$

$$T(x, 0) = T_0(x). \tag{23}$$

3. TIME DISCRETIZATION

With $\mathbf{U} = (\rho, \mathbf{w}, e)$ for the system (1)–(5) (we denote $\mathbf{w} = \rho\mathbf{u}$) or $\mathbf{U} = (\rho, \mathbf{u}, T)$ for the system (7)–(9), the unsteady problems to be solved are of the form

$$\frac{\partial \mathbf{U}}{\partial t} + G(\mathbf{U}) = 0. \tag{24}$$

We introduce fully implicit schemes, either the Euler backward scheme which is first-order accurate in time, or a Gear scheme which is second-order accurate. Let Δt (>0) be a time discretization step.

The value $\mathbf{U}_0$ being given by the initial data (21)–(23), the Euler backward scheme is described by

$$\mathbf{U}^0 = \mathbf{U}_0; \tag{25}$$

then, for $n \geqslant 0$, knowing $\mathbf{U}^n$, we compute $\mathbf{U}^{n+1}$ by

$$\frac{\mathbf{U}^{n+1} - \mathbf{U}^n}{\Delta t} + G(\mathbf{U}^{n+1}) = 0. \tag{26}$$

On the other hand, the Gear scheme is given by

$$\mathbf{U}^0 = \mathbf{U}_0, \tag{27}$$

$$\mathbf{U}^1 \quad \text{computed by (26);}$$

then, for $n \geqslant 1$, knowing $\mathbf{U}^{n-1}$ and $\mathbf{U}^n$, we compute $\mathbf{U}^{n+1}$ by

$$\frac{3\mathbf{U}^{n+1} - 4\mathbf{U}^n + \mathbf{U}^{n-1}}{2\Delta t} + G(\mathbf{U}^{n+1}) = 0. \tag{28}$$

If a steady solution is computed, a local time step is used.

4. VARIATIONAL FORMULATION

We consider the non-conservative formulation of the Navier–Stokes equations. At each time step of scheme (25), (26) or (27), (28) we have to solve a non-linear problem of the form

$$\alpha\rho + \mathbf{u}\cdot\nabla\rho + \rho\nabla\cdot\mathbf{u} = g, \tag{29}$$

$$\alpha\mathbf{u} + (\mathbf{u}\cdot\nabla)\mathbf{u} + (\gamma-1)\left(\frac{T}{\rho}\nabla\rho + \nabla T\right) - \frac{1}{Re\rho}[\Delta\mathbf{u} + \tfrac{1}{3}\nabla(\nabla\cdot\mathbf{u})] = \mathbf{f}, \tag{30}$$

$$\alpha T + \mathbf{u}\cdot\nabla T + (\gamma-1)T\nabla\cdot\mathbf{u} - \frac{1}{Re\rho}\left(\frac{\gamma}{Pr}\Delta T + F(\nabla\mathbf{u})\right) = h, \tag{31}$$

where α is a positive parameter and $\mathbf{f}$, g, h are given functions, the variables ρ, $\mathbf{u}$, T satisfying the boundary conditions (13)–(20).

We introduce the following functional spaces of Sobolev type:

$$R_r = \{\phi \mid \phi \in H^1(\Omega),\ \phi = r \text{ on } \Gamma_r\}, \tag{32}$$

with

$$\Gamma_r = \begin{cases} \Gamma_\infty & \text{if } M_\infty < 1, \\ \Gamma_\infty^- & \text{if } M_\infty \geqslant 1, \end{cases}$$

$$W_z = \{\mathbf{v} | \mathbf{v} \in (H^1(\Omega))^N,\ \mathbf{v} = \mathbf{z} \text{ on } \Gamma_B \cup \Gamma_\infty^-\}, \tag{33}$$

$$V_s = \{\theta | \theta \in H^1(\Omega),\ \theta = s \text{ on } \Gamma_B \cup \Gamma_\infty^-\}. \tag{34}$$

If r (resp. z, s) is sufficiently smooth, then R_r (resp. W_z, V_s) is non-empty (the above choice for the space of the densities R_r is motivated by the fact that ρ will be approximated by continuous functions and that the restriction of ρ to Γ_∞^- makes sense; of course, this supposes implicitly that ρ has some regularity).

Then an equivalent variational formulation of equations (29)–(31) is

$$\alpha \int_\Omega \rho\phi \mathrm{d}x + \int_\Omega (\mathbf{u} \cdot \nabla\rho)\phi + \int_\Omega \rho(\nabla \cdot \mathbf{u})\phi \mathrm{d}x = \int_\Omega g\phi \mathrm{d}x, \tag{35}$$

$$\alpha \int_\Omega \mathbf{u} \cdot \mathbf{v} \mathrm{d}x + \int_\Omega (\mathbf{u} \cdot \nabla)\mathbf{u} \cdot \mathbf{v} \mathrm{d}x + (\gamma - 1) \int_\Omega \left(\frac{T}{\rho} \nabla\rho + \nabla T \right) \cdot \mathbf{v} \mathrm{d}x - \frac{1}{Re} \int_\Omega \frac{1}{\rho} [\Delta\mathbf{u} + \tfrac{1}{3}\nabla(\nabla \cdot \mathbf{u})] \cdot \mathbf{v} \mathrm{d}x$$
$$= \int_\Omega \mathbf{f} \cdot \mathbf{v} \mathrm{d}x, \tag{36}$$

$$\alpha \int_\Omega T\theta \mathrm{d}x + \int_\Omega (\mathbf{u} \cdot \nabla T)\theta \mathrm{d}x + (\gamma - 1) \int_\Omega T(\nabla \cdot \mathbf{u})\theta \mathrm{d}x - \frac{1}{Re} \int_\Omega \frac{1}{\rho} \left(\frac{\gamma}{Pr} \Delta T + F(\nabla\mathbf{u}) \right) \theta \mathrm{d}x$$
$$= \int_\Omega h\theta \mathrm{d}x, \tag{37}$$

$$\forall \{\phi, \mathbf{v}, \theta\} \in R_0 \times W_0 \times V_0, \quad \{\rho, \mathbf{u}, T\} \in R_r \times W_z \times V_s,$$

where the values of r, z, s are determined by the boundary conditions (13)–(15) and (18)–(20).

5. SOLUTIONS OF THE NON-LINEAR PROBLEM BY PRECONDITIONED GMRES ALGORITHMS

Using appropriate finite element methods, the above non-linear system of equations is reduced to a non-linear system of finite dimension.

Among the various numerical methods which can be used for solving non-linear problems of large dimension, let us mention non-linear least-squares methods, since these methods coupled to conjugate gradient algorithms have been successfully applied to the solution of complicated problems arising from fluid mechanics (see e.g. References 1, 3 and 4 for such applications).

One of the major drawbacks of the above methods is that they require an accurate knowledge of the gradient of the cost function; for some problems this knowledge is very costly in itself (for example, this seems to be the case for the compressible Navier–Stokes equations). Recently, several investigators have introduced variants of the above methods which do not require the exact knowledge of the gradient. Among these methods, the GMRES (generalized minimal residual) algorithm[5–7] has shown interesting possibilities for non-linear problems (see References 7–9 for the theory and some applications of GMRES in fluid dynamics).

One of the first applications of the (non-linear) GMRES algorithm to non-linear problems was by Wigton *et al.*[7] They introduced an algorithm which seems quite efficient for solving some aerodynamics problems. Brown and Saad[6] have formulated this preliminary algorithm in the more general context of the inexact Newton methods and have proposed an automatic adjustment of the parameters.

We consider the non-linear problem written as

$$F(\mathbf{u}) = 0, \tag{38}$$

where F is a non-linear operator from $\mathbb{R}^N$ to $\mathbb{R}^N$.

The main idea of GMRES is to apply a basic Newton algorithm to obtain a solution of (38) and to use a linear GMRES algorithm to solve at each step a clever modification of the associated Jacobian system.

Since the costly step (in CPU time and memory storage) in the Newton algorithm is the solution of the linear system associated to the Jacobian matrix, a fruitful idea consists of obtaining an inexact solution by an iterative method, in practice the linear GMRES.[5]

Since the only operations with the Jacobian matrix $J(u)$ that are required are matrix–vector multiplications, we can make the following approximation:

$$J(u)v \simeq \frac{F(u+\sigma v)-F(u)}{\sigma},$$

where σ is some carefully chosen small scalar.[10]

Finally, we obtain the following algorithm (non-linear GMRES).

1. Start: Choose u_0 and compute $F(u_0)$. Set $n=0$.
2. Arnoldi process:
   (a) Choose a tolerance ε_n.
   (b) For an initial guess $\delta_n^{(0)}$, form $r_n^{(0)} = -F_n - J_n\delta_n^{(0)}$, where $F_n = F(u_n)$ and
   $$J_n(u)w = \frac{F(u_n+\sigma_n w)-F(u_n)}{\sigma n}.$$
   (c) Compute $\beta_n = \|r_n^{(0)}\|_2$ and $v_1 = r_n^{(0)}\beta_n$.
   (d) For $j = 1, 2, \ldots,$ do:
   $$h_{i,j} = (J_n v_j,\ v_i), \quad i = 1, 2, \ldots, j,$$
   $$\hat{v}_{j+1} = J_n v_j - \sum_{i=1}^{j} h_{i,j} v_i,$$
   $$h_{j+1,j} = \|\hat{v}_{j+1}\|_2,$$
   $$v_{j+1} = \hat{v}_{j+1}/h_{j+1,j}.$$
   (e) Compute the residual norm $\rho_j = \|F_n + J_n\delta_n^{(j)}\|_2$ of the solution $\delta_n^{(j)}$ that would be obtained if we stopped at this step.
   (f) If $\rho_j \leqslant \varepsilon_n$, set $m = j$ and go to step 3.
3. Form the approximate solution:
   (a) Define H_m to be the $(m+1)\times m$ matrix whose non-zero entries are the coefficients $h_{i,j}$, $1 \leqslant i \leqslant j+1$, $1 \leqslant j \leqslant m$, and $V_m \equiv [v_1, v_2, \ldots, v_m]$.
   (b) Find the vector y_m which minimizes $\|\beta_n e_1 - H_m y\|_2$, where $e_1 = [1, 0, \ldots, 0]^T$, over all vectors y in $\mathbb{R}^m$.
   (c) Compute $\delta_n^{(m)} = V_m y_m$ and $u_{n+1} = u_n + \delta_n^{(m)}$.
4. Stopping test: If u_{n+1} is determined to be a good enough approximation to a root of (38), then stop; else set $u_n \leftarrow u_{n+1}$, $n \leftarrow n+1$ and go to step 2.

Steps 2 and 3 of the above algorithm are precisely the linear GMRES method for solving the system $J_n\delta = -F(u_n)$.

In order to improve the convergence of the algorithm (see e.g. Reference 8), we have tested and compared different preconditioners for the solution of (38) by GMRES. We replace (38) by

$$S^{-1}F(u) = 0. \tag{39}$$

We introduce the exact Jacobian matrix of the operator F,

$$A = \partial F/\partial u, \tag{40}$$

and we use as preconditioner, S, different approximations of A, such as

$$S_1 = \text{diag}(A), \tag{41}$$

$$S_2 = (LDU)_\text{I}, \tag{42}$$

$$S_3(\varepsilon) = (LDU)_\varepsilon, \tag{43}$$

$$S_4 = LDU = A, \tag{44}$$

where we denote by diag(A) the block diagonal of A, by LDU the standard block factorization of A, by $(LDU)_\text{I}$ the incomplete one and by $(LDU)_\varepsilon$ a dynamic incomplete one.

The factorization $(LDU)_\varepsilon$ is done according to a parameter ε. While doing the factorization, the blocks (for instance of row i) are eliminated if they satisfy the absolute criterion

$$\|B_{ij}\| < \varepsilon$$

or the relative criterion

$$\|B_{ij}\| < \varepsilon \|B_{ii}\| \quad (0 \leqslant \varepsilon \leqslant 1),$$

where we define the norm $\|\cdot\|$ of a block by one of the following norms: $\|\cdot\|_1$, $\|\cdot\|_\infty$ or the classical Frobenius (or Schur's) norm $\|\cdot\|_F$.

We introduce the following sets:

$$K_1 = \{(i,j)/i \neq j\},$$

$$K_2 = \{(i,j) \text{ there is no } T \in \mathcal{T}_h \text{ such that } i \in T \text{ and } j \in T\}.$$

For the incomplete dynamic factorization of type i ($i = 1, 2$) during the Gauss factorization, we eliminate the $A_{kj}^{(k)}$ blocks satisfying $(k, j) \in K_i$ and one of the above two criteria on B_{ij}.

With this notation we can see the type 1 factorization as an enrichment of diag(A) and the type 2 as an enrichment of $(LDU)_\text{I}$.

For more details concerning the preconditions see Reference 20.

Remark 1

For the incomplete factorization $(LDU)_\text{I}$ we make the Gauss factorization using only the blocks $A_{ij}^{(k)}$ with $(i,j) \in K_2$.

Remark 2

In the case of the relative test we have

$$S_3^i(0) = S_4, \quad i = 1, 2,$$

$$S_3^1(1) = S_1,$$

$$S_3^2(1) = S_2.$$

6. COMPATIBLE FINITE ELEMENT APPROXIMATIONS

It is well known that for the incompressible Navier–Stokes equations, pressure and velocity cannot be approximated independently (see e.g. Reference 11 and references therein).

Concerning now the compressible Navier–Stokes equations, there has been a natural tendency to use the same approximation for all variables, the numerical viscosity of the scheme (due to upwinding, artificial viscosity, viscosity introduced via time discretization, etc.) being generally sufficient to obtain solutions without oscillations.

Our aim was, in view of accuracy, to explore the possibility of using a centred Galerkin scheme without any viscosity added, at least for moderate Reynolds numbers and for solutions without sharp shocks.

With the same piecewise linear continuous approximations for all variables we have obtained satisfying results using the Glowinski–Pironneau solver for the solution of the generalized Stokes problem,[12] which is a subproblem of the Navier–Stokes equations. This method implies more regularity on the density than, for instance, a Hood–Taylor method; this explains why we obtain smooth solutions with the Glowinski–Pironneau solver and spurious oscillations if a Hood–Taylor method is used.

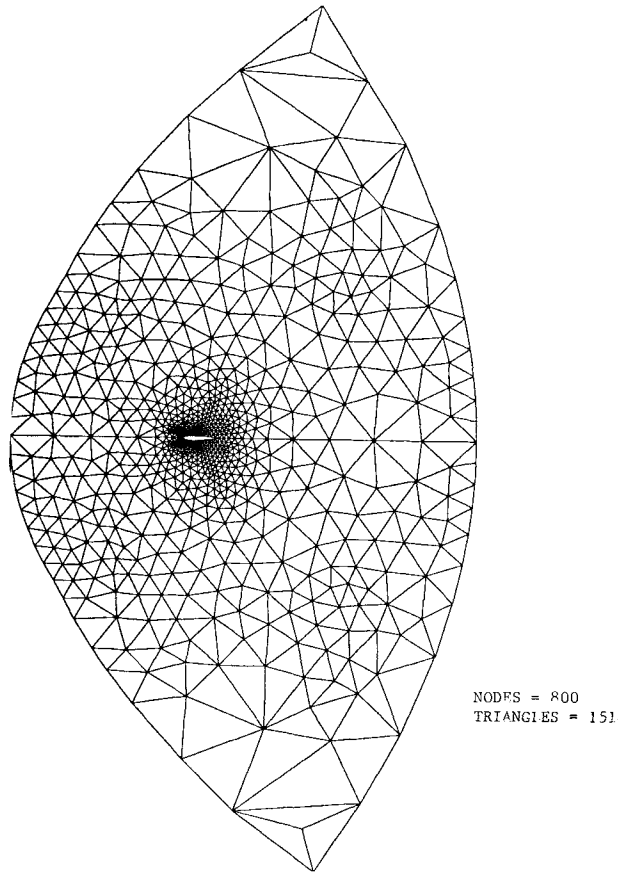

Figure 2. Coarse triangulation T_h around NACA0012

The same oscillations appear if we solve the Navier–Stokes system by the algorithm defined in Section 5 with the same approximations for all the variables.

Let T_h be a standard finite element triangulation of Ω. We introduce the following discrete spaces (with P_k = space of polynomials of degree $\leqslant k$):

$$R_{rh} = \{\phi_h | \phi_h \in C^0(\bar{\Omega}),\ \phi_h|_T \in P_1,\ \forall T \in T_h,\ \phi_h = r_h \text{ on } \Gamma_h\}, \tag{45}$$

$$W_{zh} = \{\mathbf{v}_h | \mathbf{v}_h \in (C^0(\bar{\Omega}))^2,\ \mathbf{v}_h|_T \in P_1 \times P_1,\ \forall T \in T_h,\ \mathbf{v}_h = \mathbf{z}_h \text{ on } \Gamma_B \cup \Gamma_\infty^-\}, \tag{46}$$

$$V_{sh} = \{\theta_h | \theta_h \in C^0(\bar{\Omega}),\ \theta_h|_T \in P_1,\ \forall T \in T_h,\ \theta_h = s_h \text{ on } \Gamma_B \cup \Gamma_\infty^-\}. \tag{47}$$

Then we can write for the discrete problem the algorithm previously defined for the continuous one.

We have considered as a test case the flow around an NACA0012 aerofoil. We have used first the triangulation (800 nodes, 1514 triangles) shown in Figure 2. The test case is a transonic calculation at $M_\infty = 0{\cdot}8$, $Re = 73{\cdot}0$, at an angle of attack of 10°. The density contours exhibit spurious oscillations as shown in Figure 3.

Let $\tilde{T}_h$ be the triangulation deduced from T_h by joining the midpoints of the edges of $T \in T_h$. We have computed the same test case with T_h replaced by $\tilde{T}_h$ (as shown in Figure 4). We find again the same kind of oscillations on the density contours (Figure 5).

These oscillations look like the checkerboard oscillations of pressure which appear when the same approximations are used for the pressure and velocity variables to solve the incompressible Navier–Stokes equations.

Figure 3. Density contours. P_1 approximations on the coarse mesh for all variables

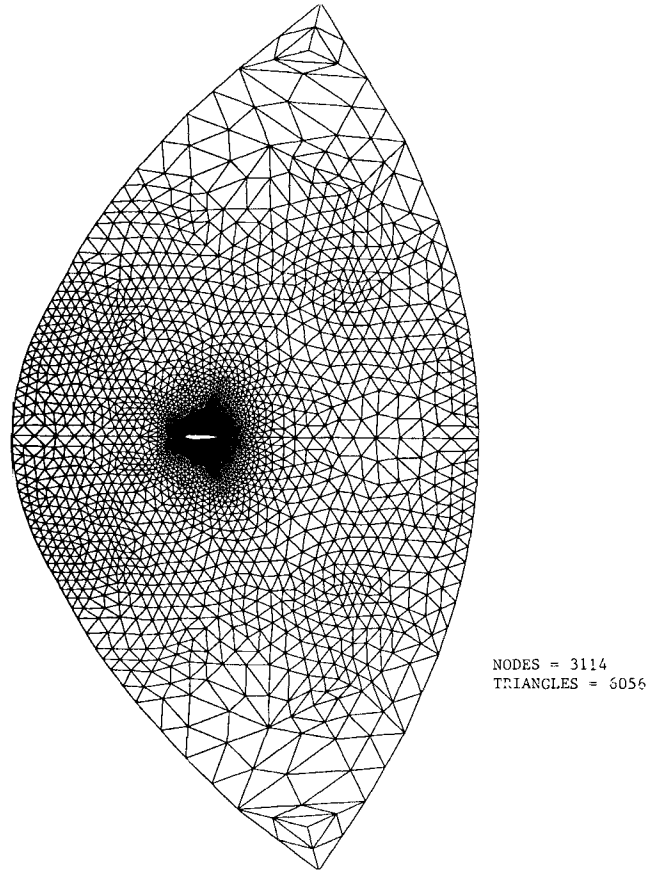

Figure 4. Fine triangulation $\tilde{T}_h$ around NACA0012

We have considered the following equations:

$$\alpha\rho + \nabla \cdot \mathbf{u} = g, \tag{48}$$

$$\alpha\mathbf{u} - \mu\Delta\mathbf{u} + \nabla\rho = 0, \tag{49}$$

$$\mathbf{u} = 0 \quad \text{on } \Gamma.$$

This system is a subproblem of (29), (30) (or of (30), (31) with ρ replaced by T) and is a 'generalized' Stokes problem.

If we solve this problem with the discrete spaces defined by (45), (46) we also obtain oscillating solutions (see Figure 6 for an example with $\alpha = 1$, $\mu = 0{\cdot}01$ and all the variables approximated on a triangulation of 3114 nodes; the figure shows the density contours).

We define

$$\tilde{W}_{zh} = \{\mathbf{v}_h | \mathbf{v}_h \in (C^0(\bar{\Omega}))^2,\ \mathbf{v}_h|_{\tilde{T}} \in P_1 \times P_1,\ \forall \tilde{T} \in \tilde{T}_h,\ \mathbf{v}_h = \mathbf{z}_h \text{ on } \Gamma_B \cup \Gamma_\infty^-\}. \tag{50}$$

Then, if we choose

$$\rho_h \in R_{rh}, \qquad \mathbf{u}_h \in \tilde{W}_{zh},$$

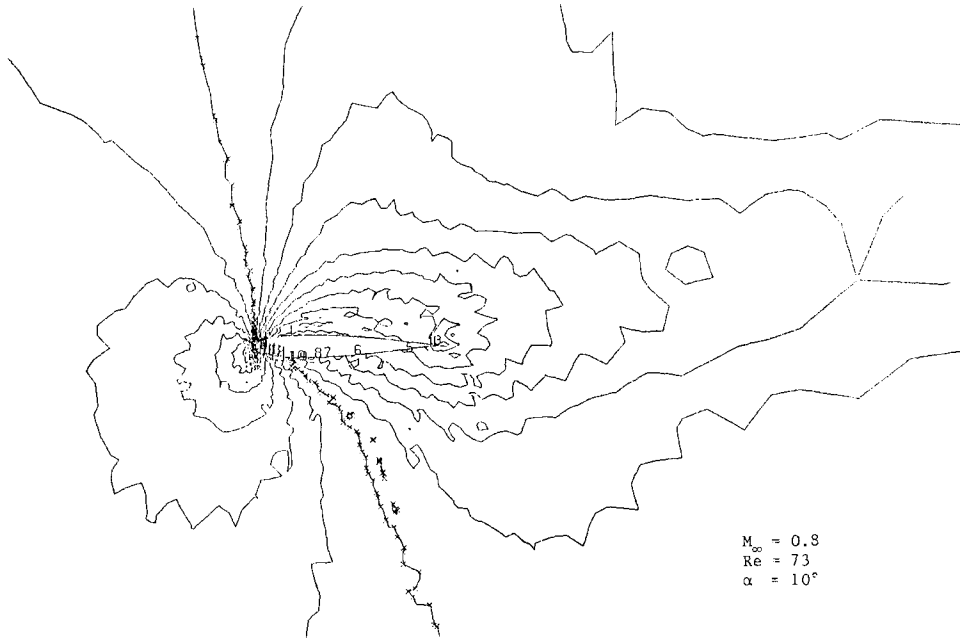

Figure 5. Density contours. P_1 approximations on the fine mesh for all variables

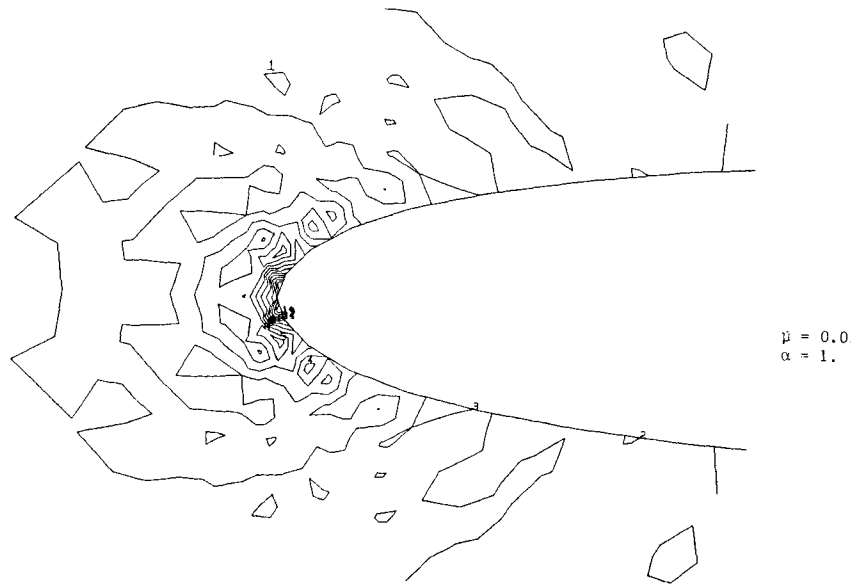

Figure 6. Density contours. Simplified problem. P_1 approximations on the fine mesh for all variables

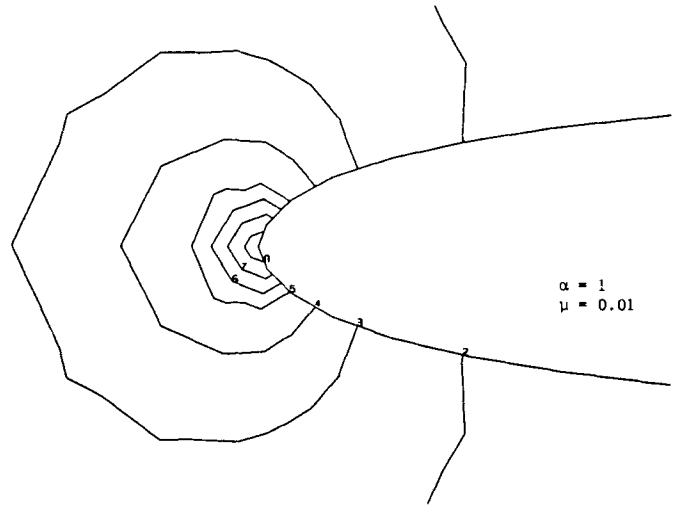

Figure 7. Density contours. Simplified problem. Compatible approximations

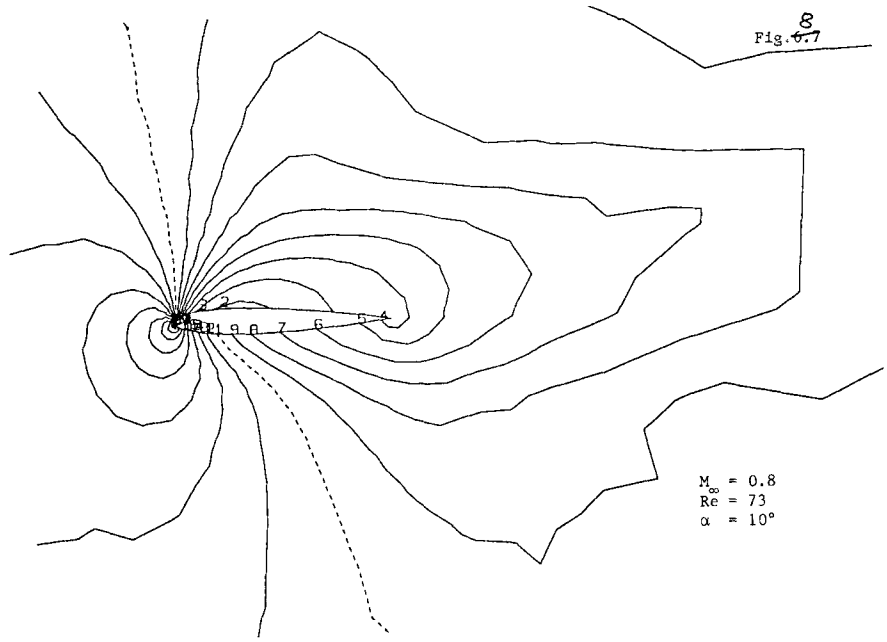

Figure 8. Density contours. P_1, P_1–iso-P_2 approximations

we obtain for problem (48), (49) the satisfying solution shown in Figure 7 (with the triangulation for T_h presented on Figure 2).

This result tends to prove numerically that for problem (48), (49) a compatibility condition (some inf-sup condition[13]) has to be satisfied by the approximations of the different variables.

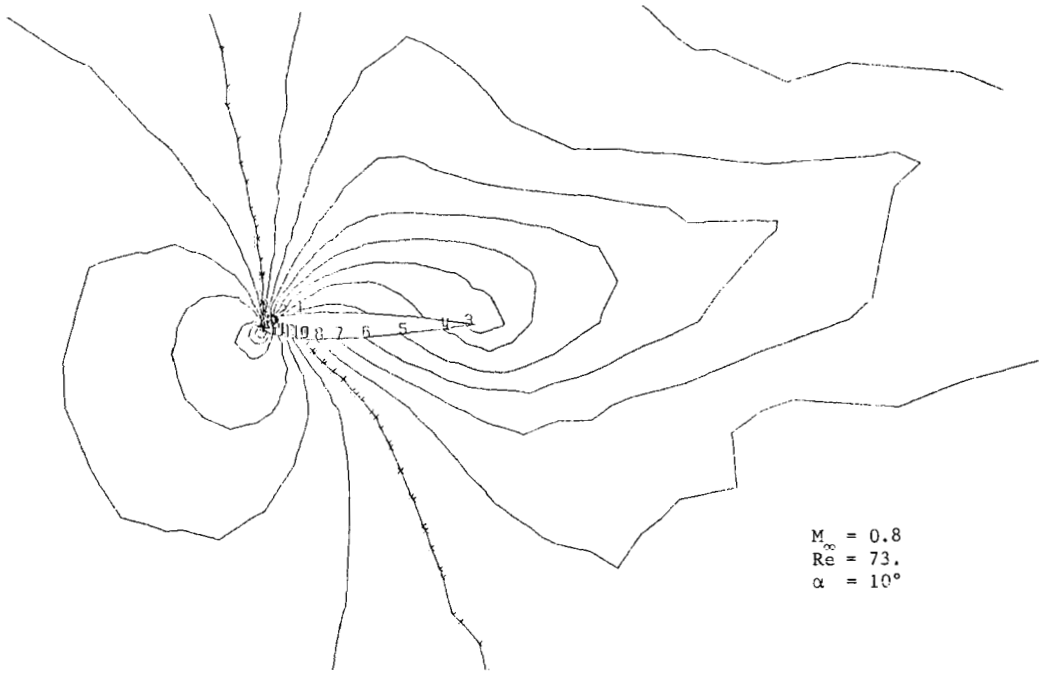

Figure 9. Density contours. P_1, P_1 + bubble approximations

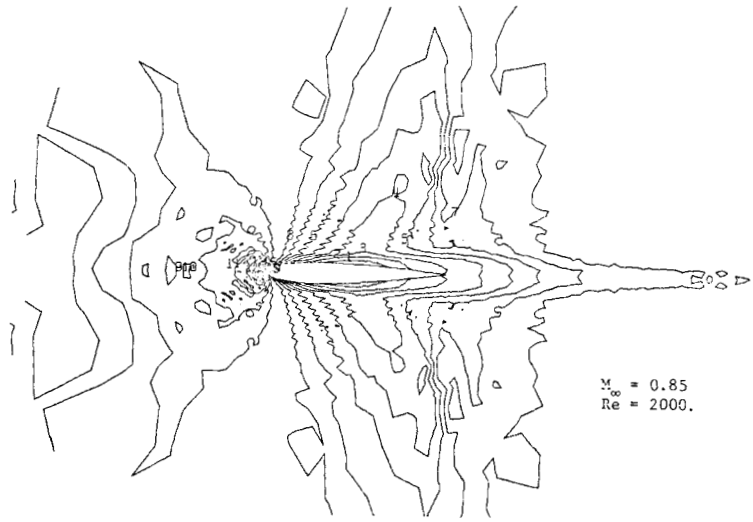

Figure 10. Density contours. P_1 approximations for all variables

Concerning the compressible Navier–Stokes equations (Sections 2–4), if we consider the test case previously defined with $\rho_h \in R_{rh}$, $T_h \in V_{sh}$ and $\mathbf{u}_h \in \tilde{W}_{zh}$, we also obtain good results for the density contours, as shown in Figure 8. We will denote this approximation by 'P_1, P_1–iso-P_2' (the velocity has the same number of degrees of freedom as with a P_2 approximation).

We can also replace $\tilde{W}_{zh}$ by (this space has been introduced in Reference 14)

$$\bar{W}_{zh} = \{\mathbf{v}_h | \mathbf{v}_h \in (C^0(\bar{\Omega}))^2,\ \mathbf{v}_h|_T \in P^*_{1T} \times P^*_{1T},\ \forall T \in T_h\}. \tag{51}$$

In (51), P^*_{1T} is the subspace of P_3 defined as follows:

$$P^*_{1T} = \{q | q = q_1 + \lambda \phi_T, \text{ with } q_1 \in P_1,\ \lambda \in R, \text{ and } \phi_T \in P_3,\ \phi_T = 0 \text{ on } \partial T,\ \phi_T(G_T) = 1\}, \tag{52}$$

where G_T is the centroid of T. A function like ϕ_T is usually called a bubble function.

If we choose $\rho_h \in R_{rh}$, $T_h \in V_{sh}$, $\mathbf{u}_h \in \bar{W}_{zh}$, a good solution is also computed as shown in Figure 9. We will denote this approximation by 'P_1, P_1 + bubble'.

Concerning the conservative formulation (1)–(5), some first results prove also the interest of compatible approximations to avoid oscillations.

Some other results are presented in Section 7. They prove numerically that accurate solutions can be computed by a centred scheme as soon as a compatibility condition is satisfied by the approximations of the different variables (see also Reference 21).

Some theoretical results have been proved on simplified model problems by Pironneau and Rappaz for adiabatic stationary flows[2] and by Fortin and Soulaimani.[15]

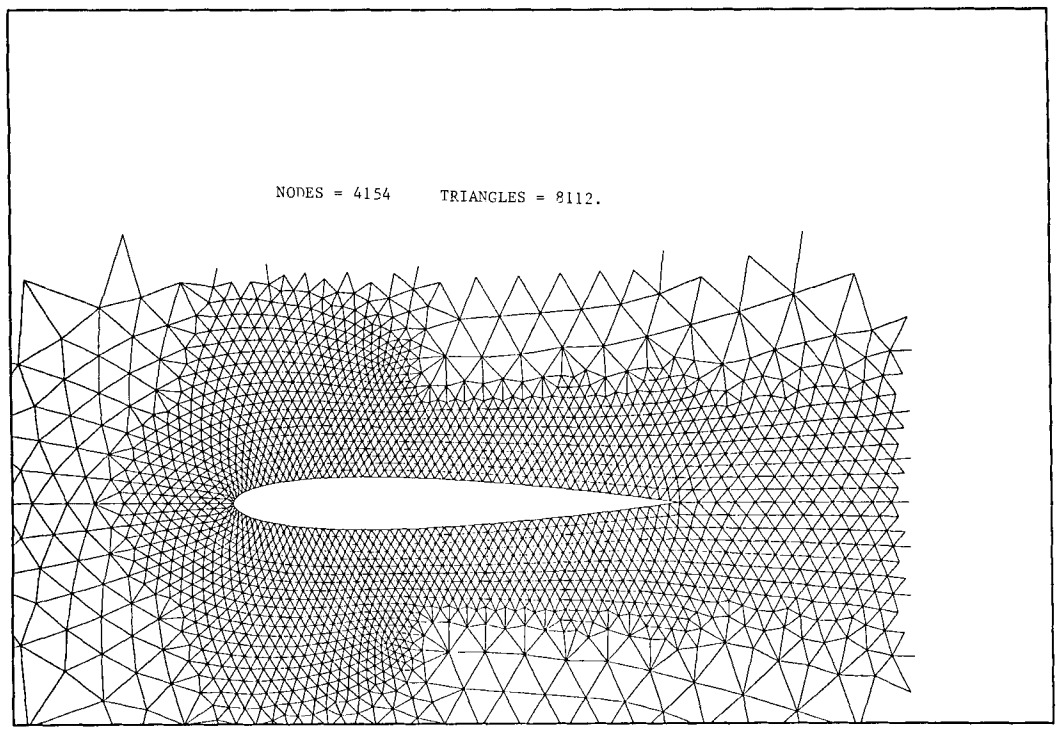

Figure 11. Enlargement of a triangulation around NACA0012

7. NUMERICAL RESULTS

In this section we present some more 2D and 3D results to assess the accuracy and efficiency of the method.

The first result concerns a two-dimensional transonic flow around an NACA0012 at $M_\infty = 0{\cdot}85$, $Re = 2000$, a test case of the compressible Navier–Stokes workshop held in Nice in 1985.[16] With the same P_1 approximations for all variables we obtain again an oscillating solution as shown in Figure 10; therefore we have used the P_1, P_1–iso-P_2 and the P_1, P_1 + bubble approximations of Section 6. With the first type of approximations and the mesh shown in Figure 11 for the density and the temperature, we have computed the solution described in Figures 12–14 by the density contours, the Mach contours and the pressure coefficient on the body respectively.

For the second type of approximations we have used the adapted mesh[17–19] shown in Figure 15. The criterion (depending on the solution computed on the mesh of Figure 11) used to choose the area to be refined is

$$\frac{\mathbf{u} \times \nabla M}{|\mathbf{u}|},$$

where M is the local Mach number. Figure 16 shows the Mach contours and Figure 17 the skin friction coefficient.

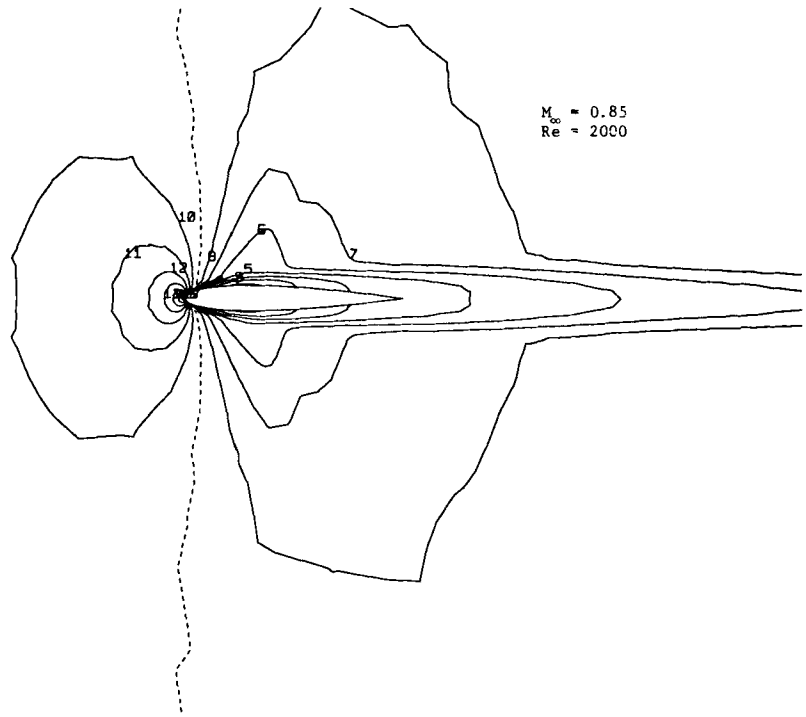

Figure 12. Density contours. P_1, P_1–iso-P_2 approximations

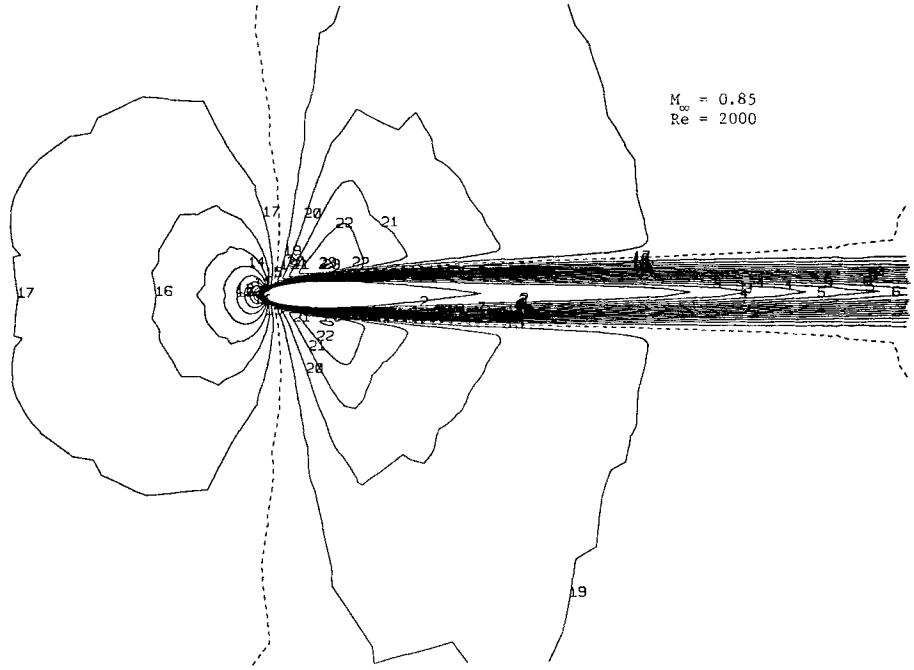

Figure 13. Mach contours. P_1, P_1–iso-P_2 approximations

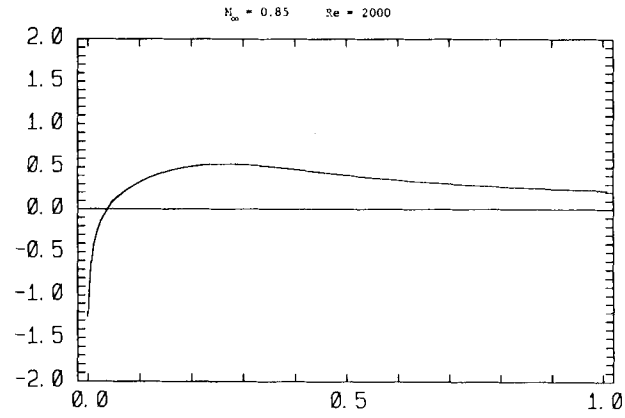

Figure 14. Pressure coefficient on the wall. P_1, P_1–iso-P_2 approximations

With the two types of approximations, the results are in very good agreement with the results issued from the workshop and which can be considered as references.

The second case deals with an unsteady flow computed with $M_\infty = 0{\cdot}6$, $Re = 5 \times 10^3$, $\alpha = 10°$. The time step is $\Delta t = 0{\cdot}05$. Starting from the free-stream solution, we obtain at about $t = 7$ the solution described by the Mach contours of Figure 18, the isobar contours of Figure 19 and the

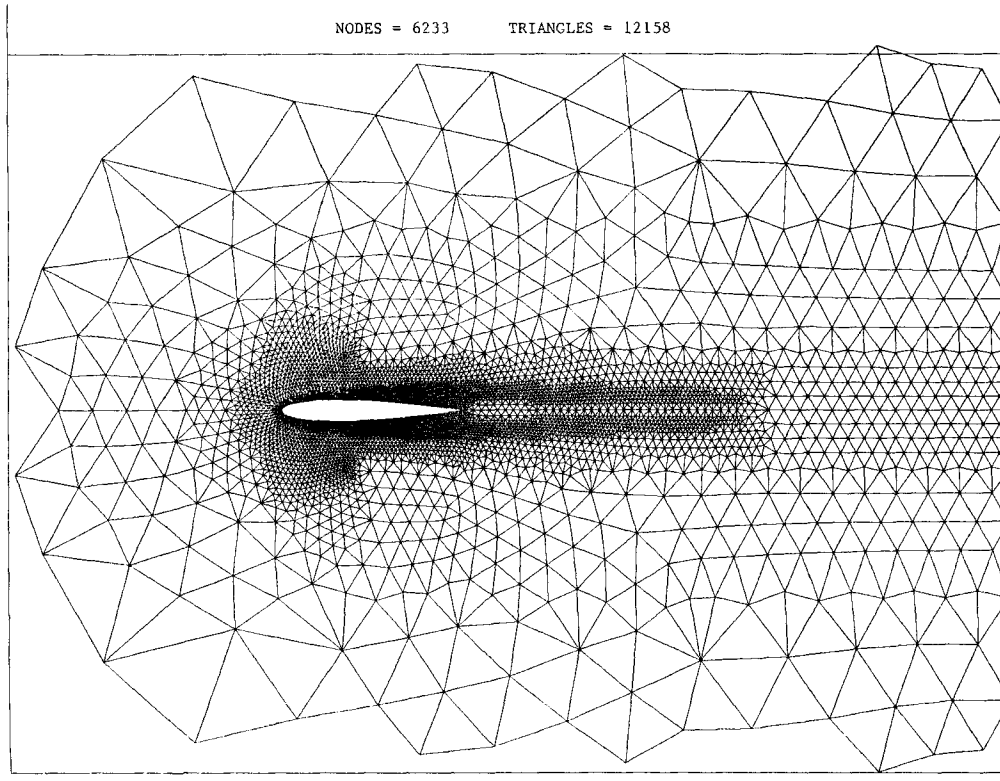

Figure 15. Enlargement of a triangulation around NACA0012

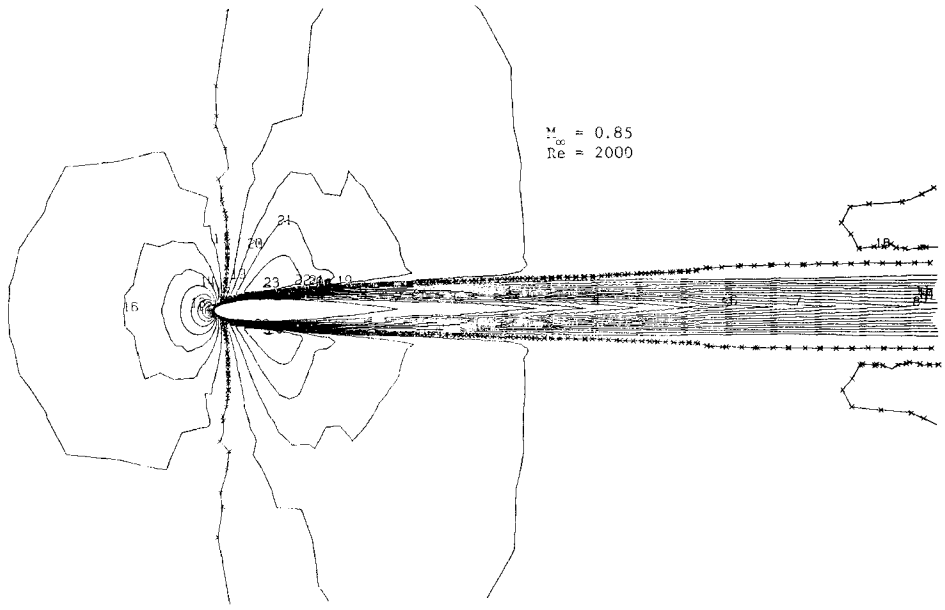

Figure 16. Mach contours. P_1, P_1 + bubble approximations

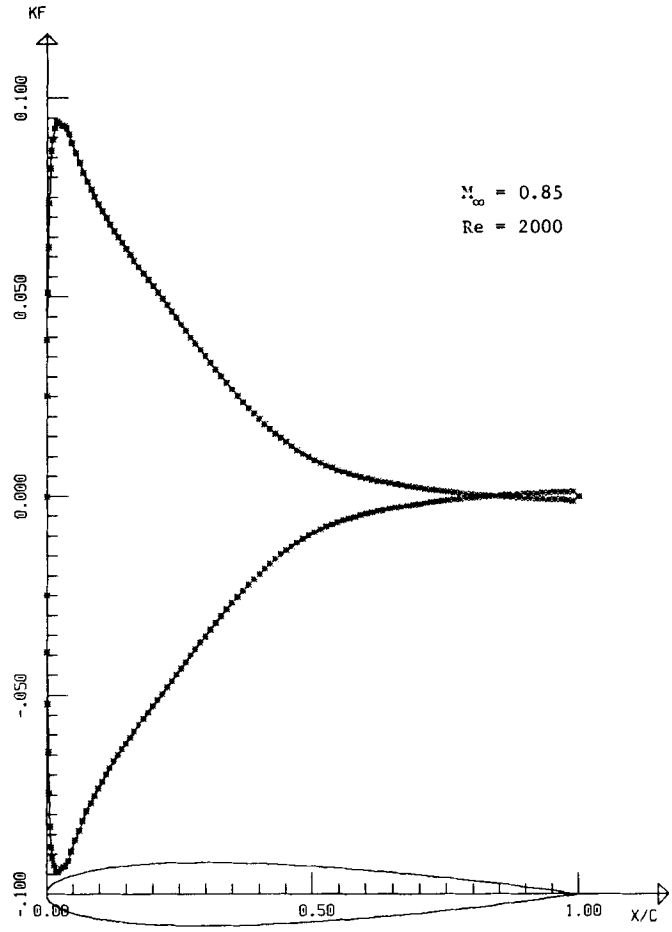

Figure 17. Skin friction coefficient. P_1, P_1 + bubble approximations

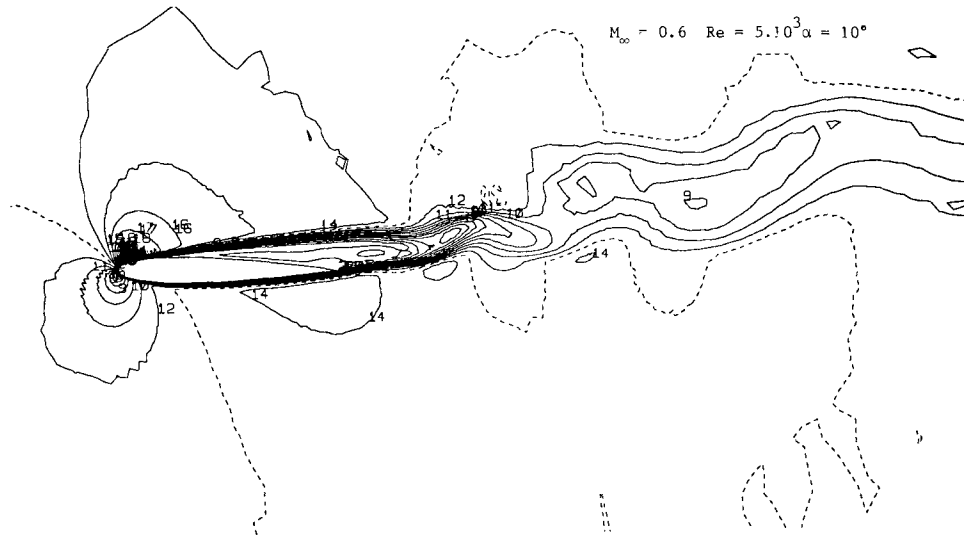

Figure 18. Mach contours

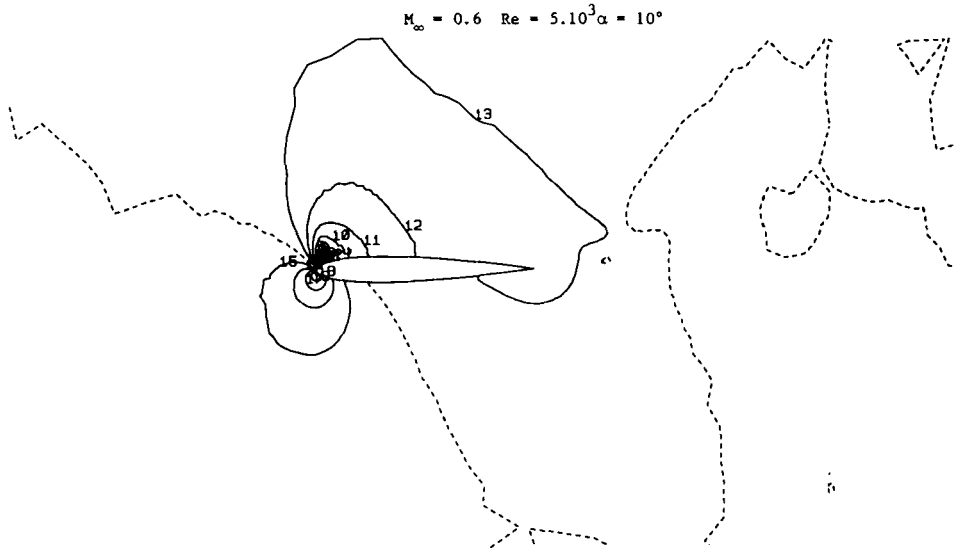

Figure 19. Isobar contours

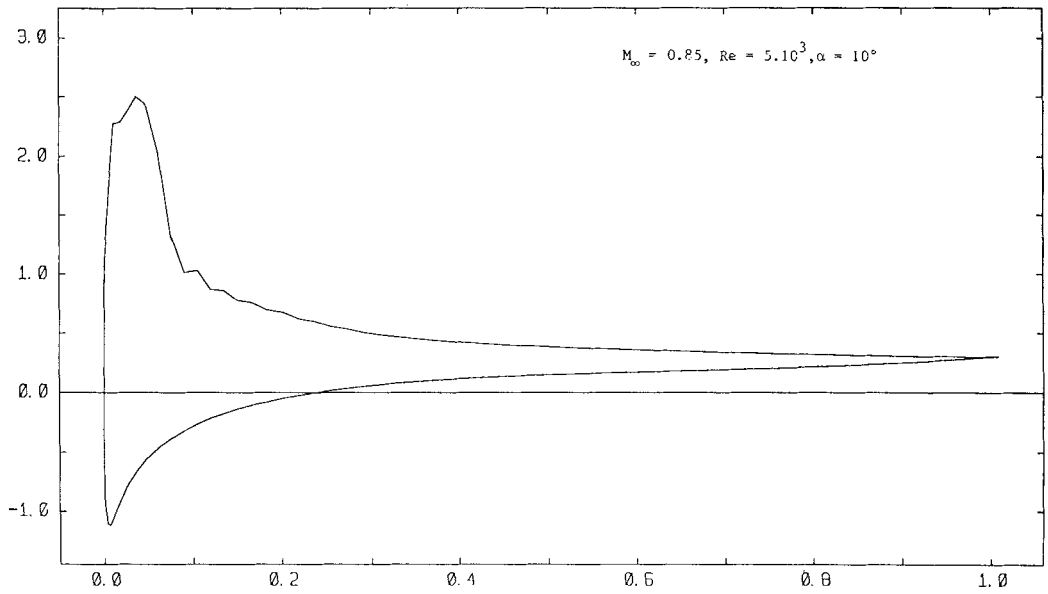

Figure 20. Pressure coefficient on the wall

pressure coefficient on the wall of Figure 20. The P_1, P_1–iso-P_2 approximation was used for this simulation with the mesh of Figure 11.

The following example concerns a supersonic computation, which has been computed on an automatically adapted mesh (Figure 21); the physical criterion used to choose the area to be

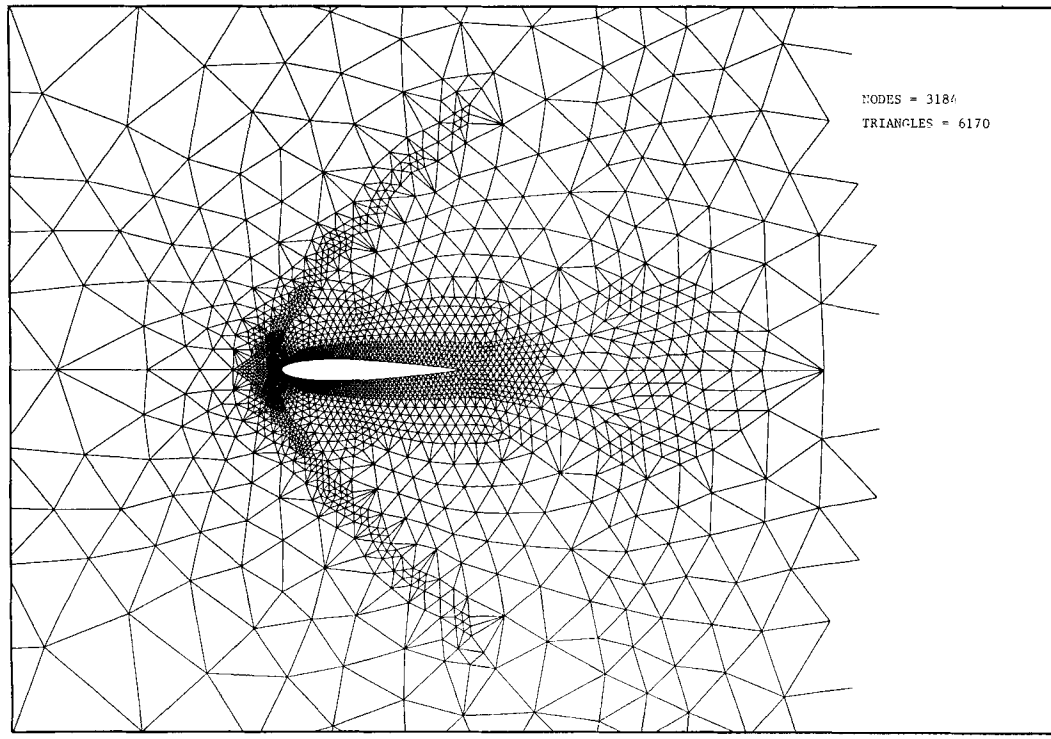

Figure 21. Enlargement of an adapted mesh around NACA0012

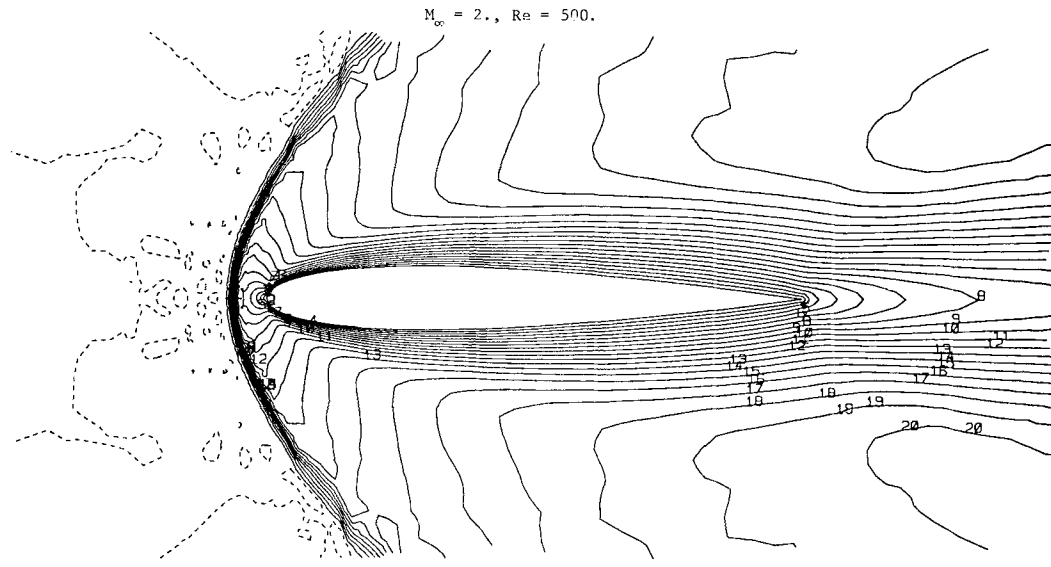

Figure 22. Mach contours

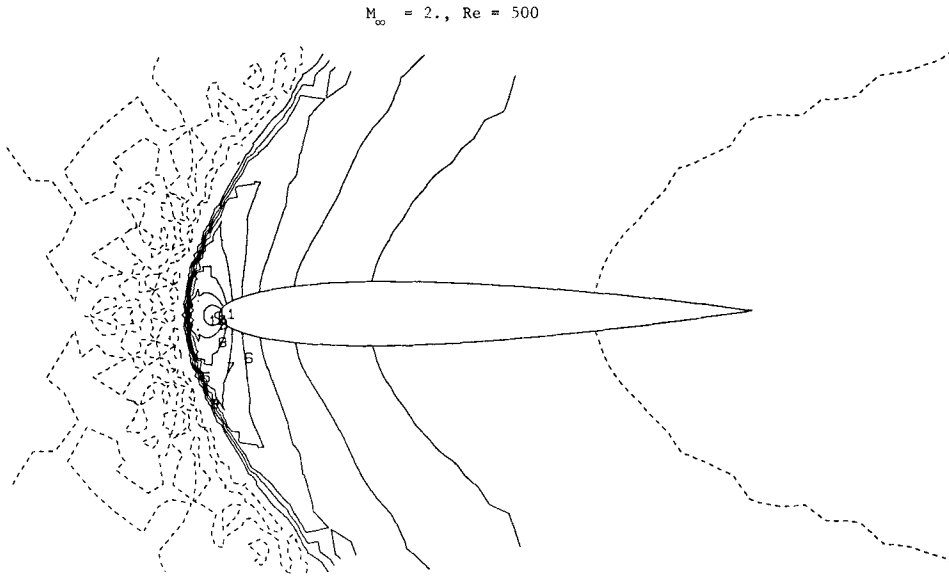

Figure 23. Isobar contours

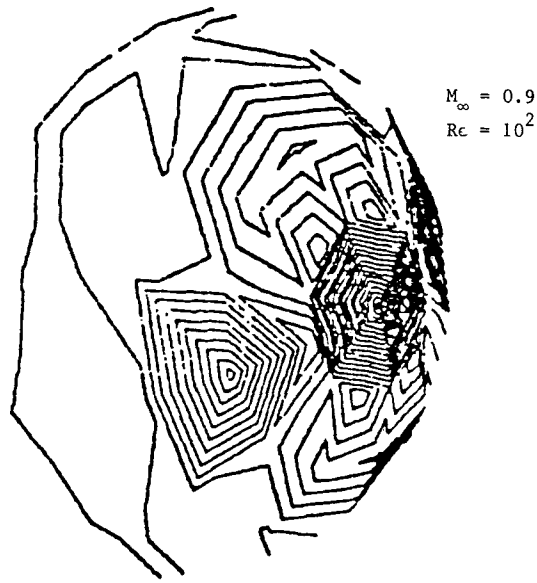

Figure 24. P_1 approximations

refined is the gradient of temperature.[17–19] The test case is $M_\infty = 2$, $Re = 500$. Figure 22 shows the Mach contours and Figure 23 the isobar contours.

In order to show also the necessity of compatible approximations for three-dimensional calculations, Figures 24 and 25 compare the density contours of the flow around a sphere using the

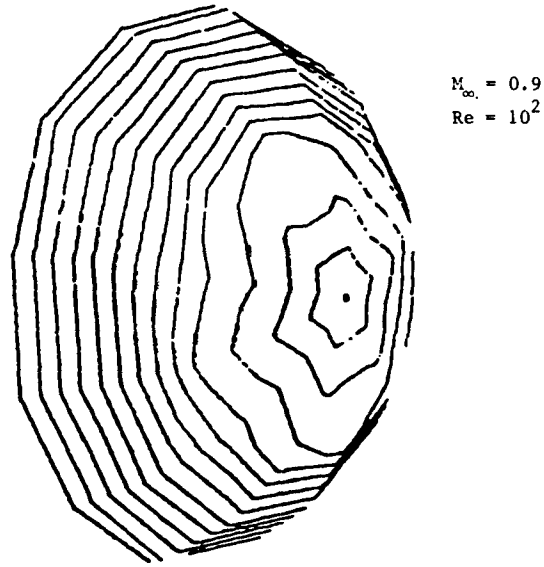

Figure 25. P_1, P_1 + bubble approximations

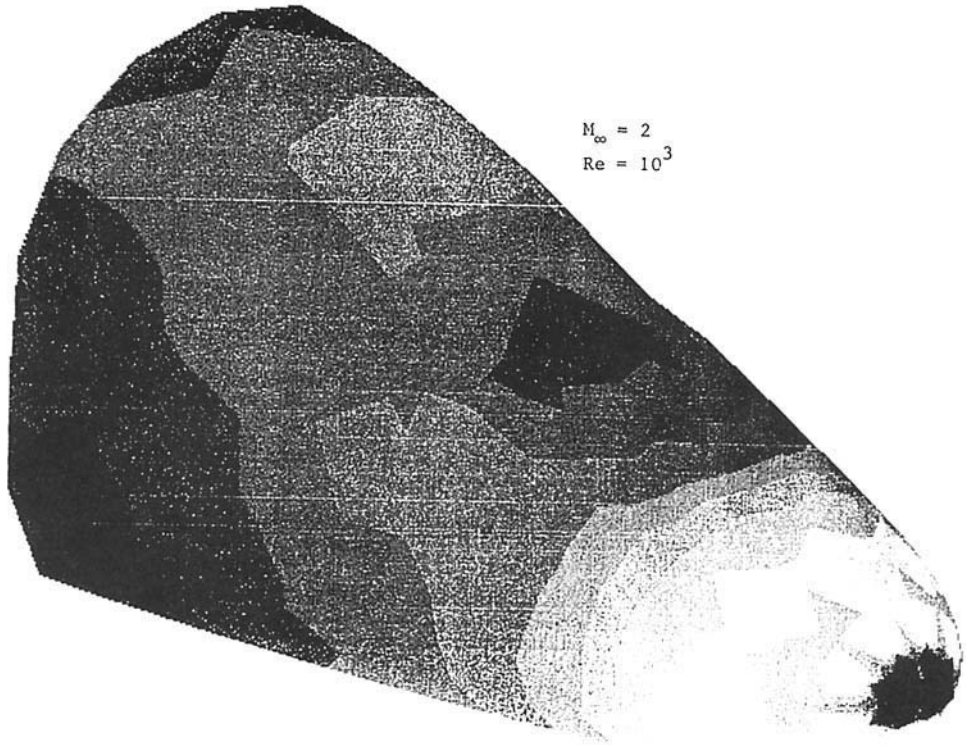

Figure 26. Pressure coefficient. P_1 approximations

P_1 approximations of the P_1, P_1 + bubble approximations. The test case is $M_\infty = 0{\cdot}9$, $Re = 10^2$. The second 3D result concerns a flow close to the forebody of the space vehicle Hermes at $M_\infty = 2$, $Re = 10^3$. Figure 26 shows the oscillating pressure coefficient obtained with the P_1 approximations and Figure 27 shows the (rather coarse) mesh on the body and the pressure coefficient obtained with the P_1, P_1 + bubble approximations.

The remaining results concern the acceleration of the convergence of the non-linear GMRES algorithm.

We have considered three test cases concerning a two-dimensional flow around an elliptic body at $M_\infty = 0{\cdot}8$. The time step is $\Delta t = 0{\cdot}05$ and the dimension of the Krylov space is four. For the first test case, at $Re = 10^3$, we use the P_1, P_1–iso-P_2 approximations with a mesh of 840 nodes for the density and the temperature. For the second test case, at the same Reynolds number, we use the P_1, P_1 + bubble approximations with the mesh defined for the velocity in the previous case (3280 nodes), for the density and the temperature. The last test case deals with the same approximations on the coarse mesh (840 nodes) at $Re = 10^2$.

Figures 28–37 study the convergence of the preconditioned GMRES algorithm to solve the non-linear system at the 11th time step.

Figures 28–30 show the efficiency of the preconditioner $S_3^1(\varepsilon)$ according to the value of the parameter ε for the first test case; for different values of ε we study the requested memory, the number of iterations and the CPU time. In Figure 28 the number of coefficients of the matrix $S_3^1(\varepsilon)$

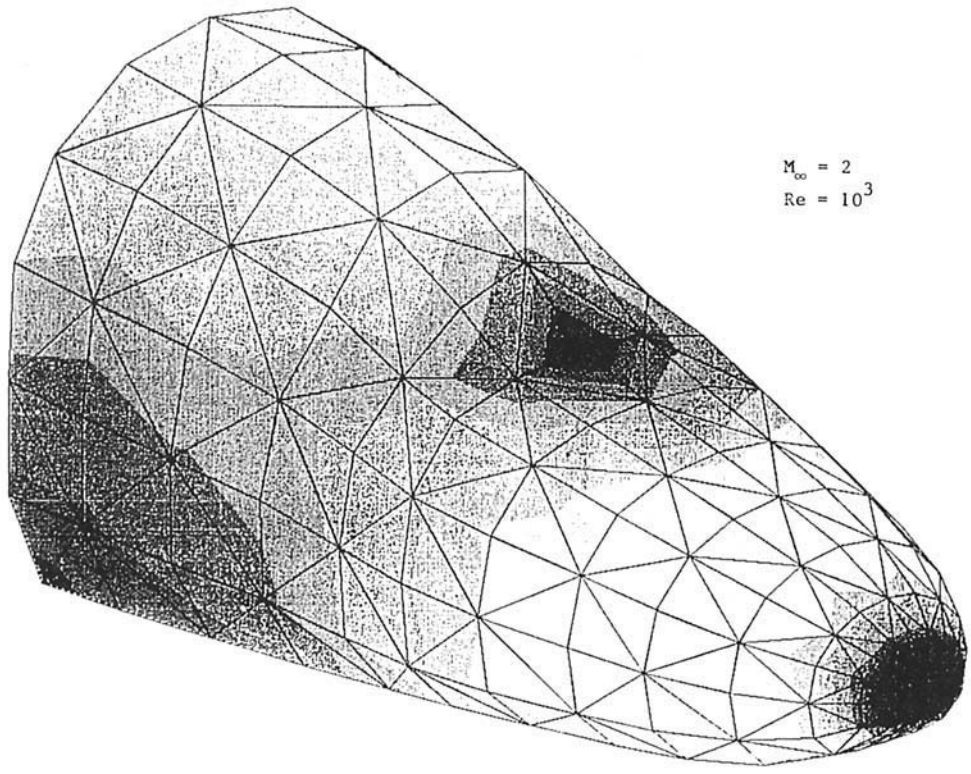

Figure 27. Pressure coefficient. P_1, P_1 + bubble approximations

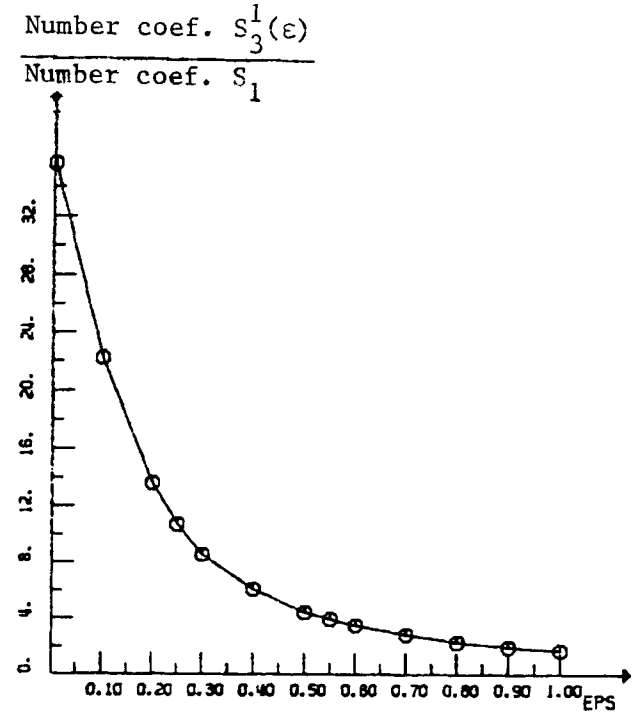

Figure 28. Requested memory versus ε

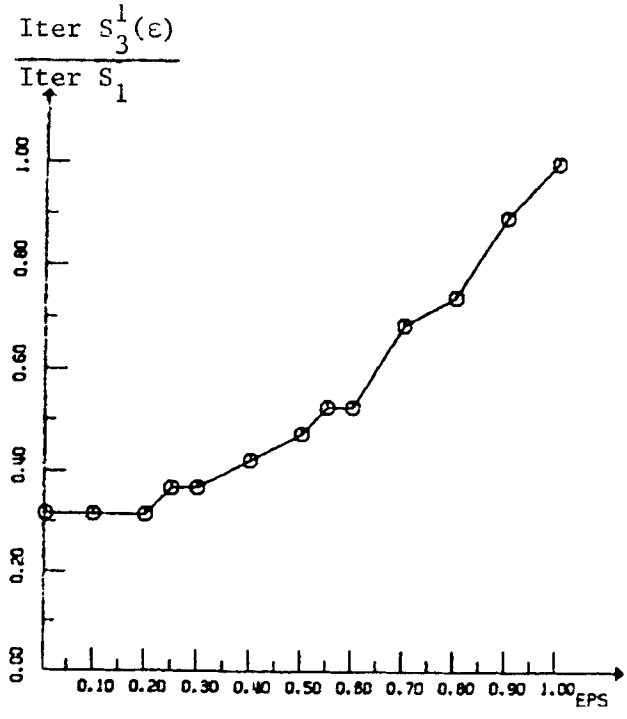

Figure 29. Number of iterations versus ε

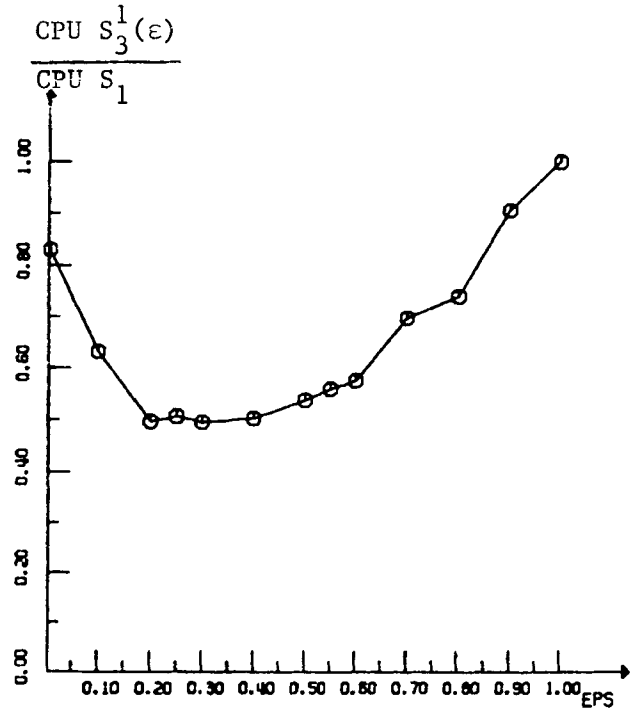

Figure 30. CPU time versus ε

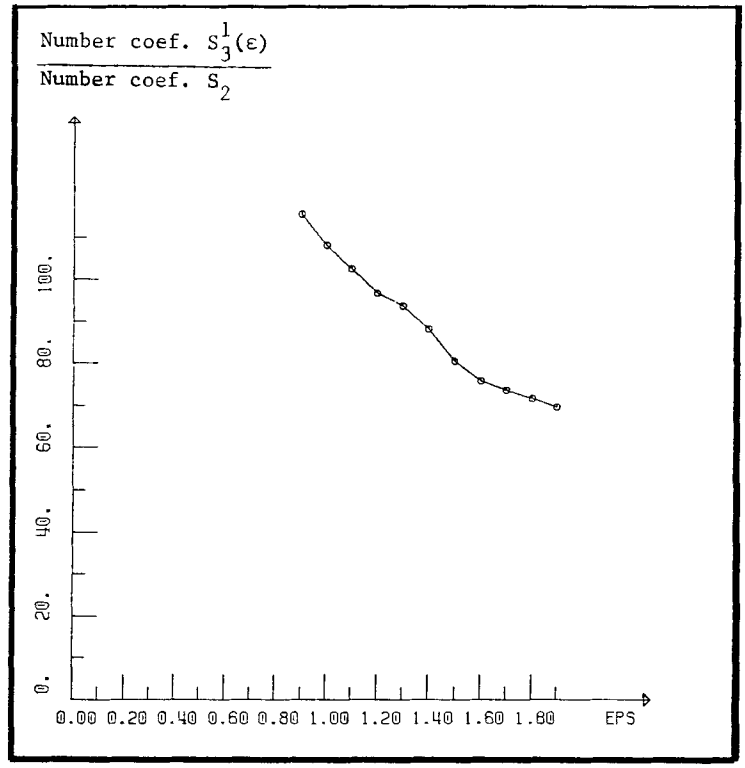

Figure 31. Requested memory versus ε

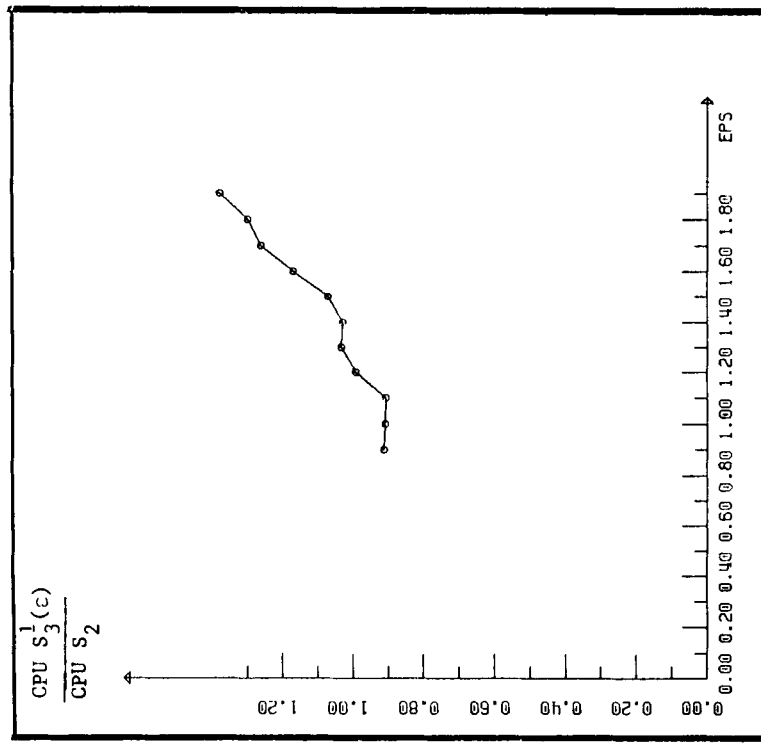

Figure 33. CPU time versus ε

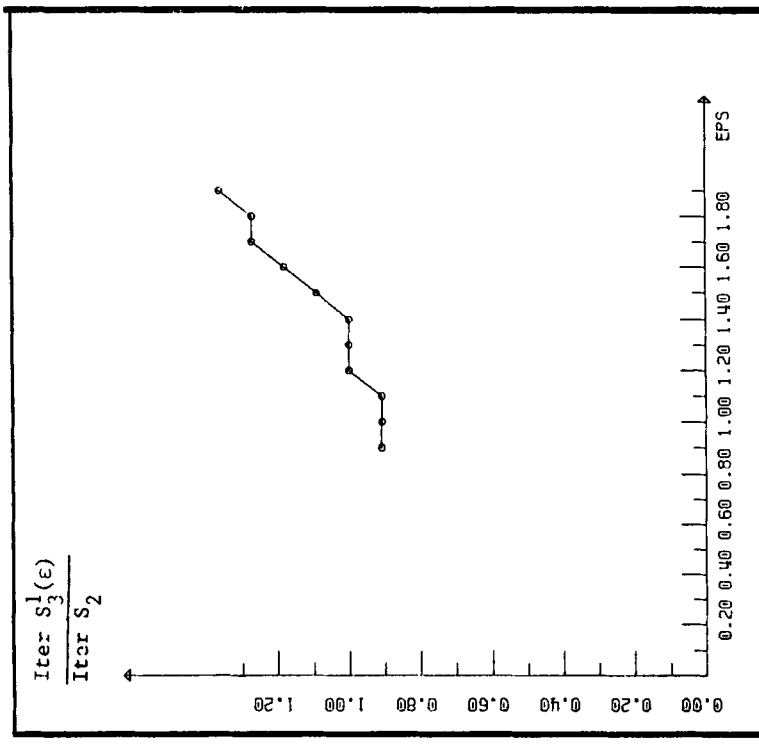

Figure 32. Number of iterations versus ε

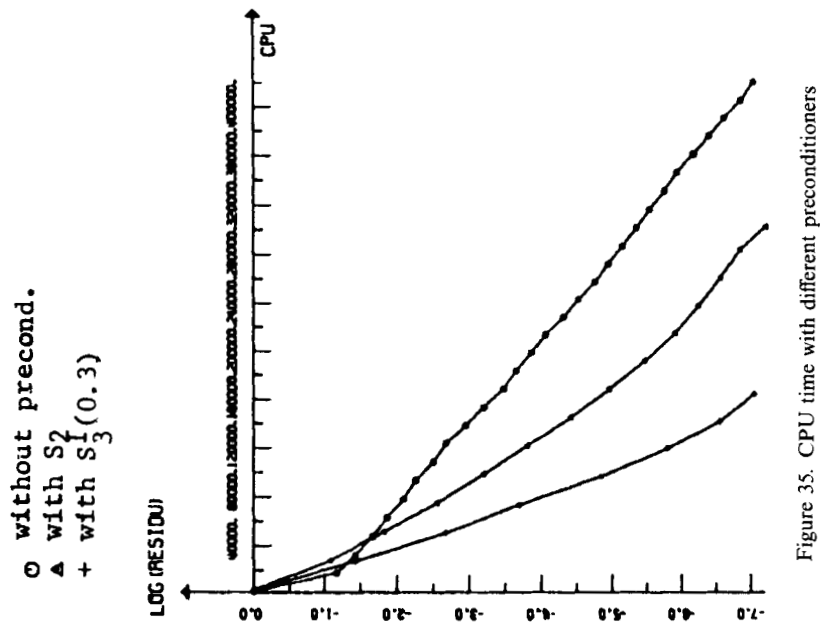

Figure 35. CPU time with different preconditioners

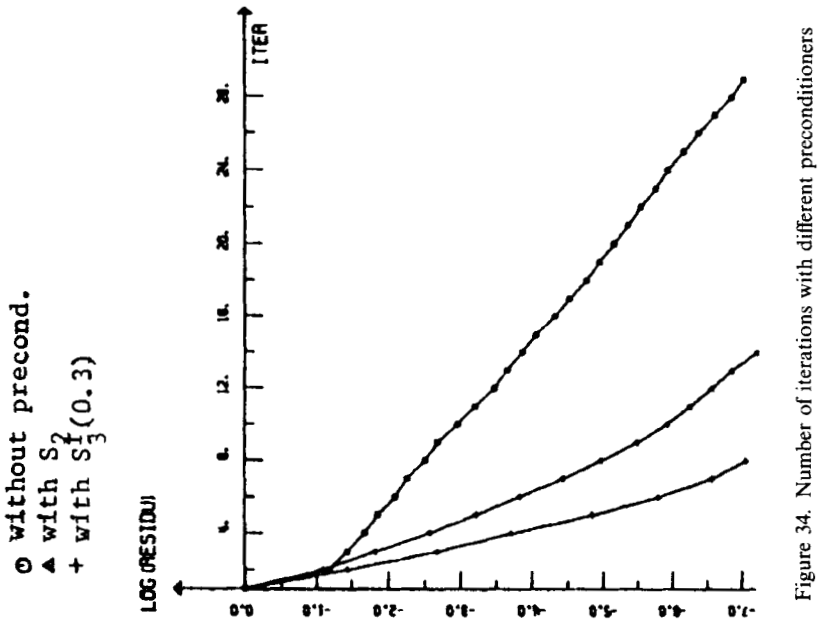

Figure 34. Number of iterations with different preconditioners

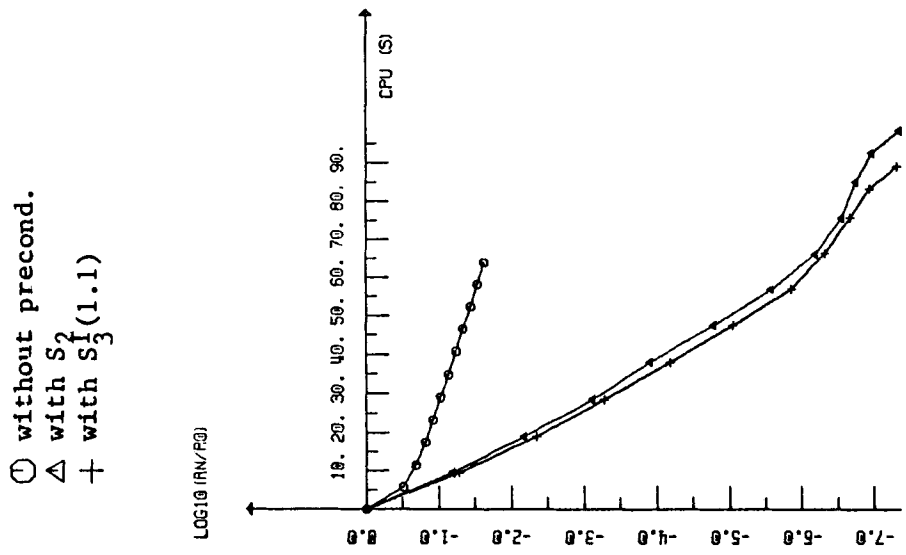

Figure 37. CPU time with different preconditioners

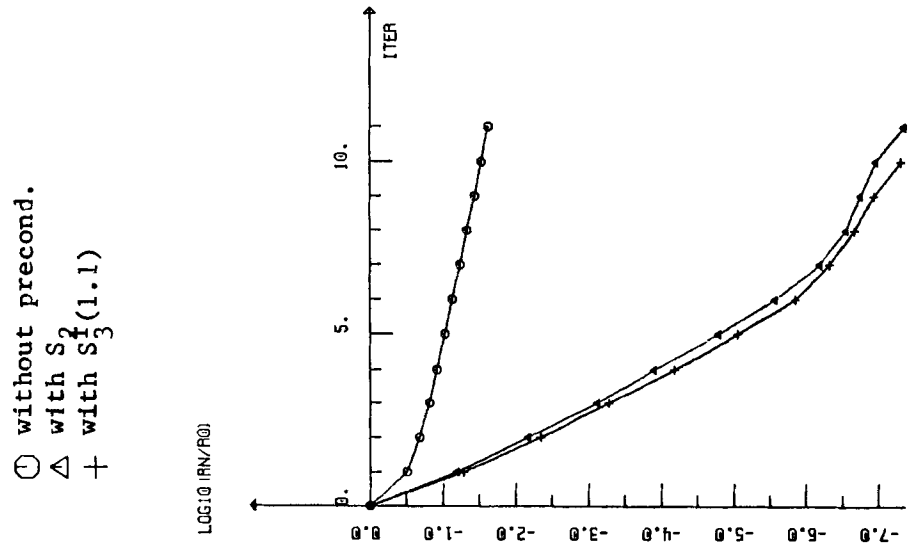

Figure 36. Number of iterations with different preconditioners

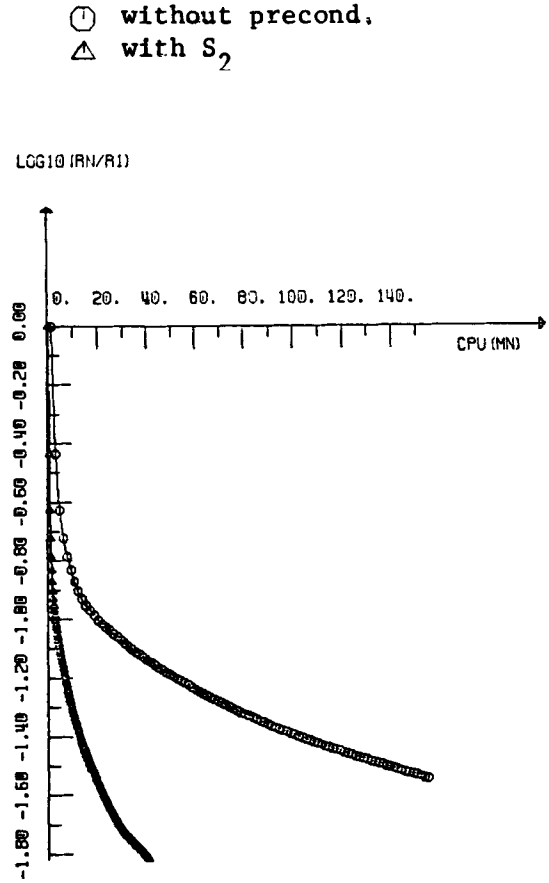

Figure 38. Convergence history of the global algorithm

is related to the number of coefficients of S_1 (we have used the absolute criterion and Schur's norm). In Figure 29 the number of iterations obtained with $S_3^1(\varepsilon)$ is related to the number of iterations obtained with S_1. In Figure 30 the CPU time obtained with $S_3^1(\varepsilon)$ is related to the CPU time obtained with S_1. The results obtained with S_2 are shown by the solid lines. We deduce that for this test case the value $\varepsilon = 0{\cdot}3$ is nearly optimal: it uses the same storage as S_2 and the CPU time is divided by two.

The same study has been done for the second test case with $S_3^1(\varepsilon)$ compared to S_2. The results concerning the number of coefficients of the matrix, the number of iterations and the CPU time are shown in Figures 31–33 respectively. For this test case the value $\varepsilon = 1{\cdot}1$ can be taken as optimal, with a smaller variation from the results obtained with S_2 than in the previous case.

In the following figures we compare the convergence history of the algorithm without preconditioner and with the preconditioners S_2 and $S_3^1(\varepsilon)$ (with the optimal value of ε). Figures 34 and 35 show for the first test case the convergence histories in terms of the number of iterations and the CPU time on an IBM 4381 respectively. The Figures 36 and 37 show the corresponding plots for the second test case. These curves show the efficiency of the preconditionings. Note that the CPU times necessary for matrix construction and factorization are not taken into account since they do not have to be done at each time step.

Finally, in Figure 38 we show for the last test case the convergence history of the global algorithm (25), (26) using at each time step the GMRES algorithm without preconditioner or with the S_2 preconditioner.

8. CONCLUSIONS

We have discussed in this paper the numerical simulation of compressible viscous flow by a methodology combining finite elements for the space discretization, an implicit second-order multistep scheme for the time discretization and a preconditioned GMRES iterative algorithm for the solution of the finite-dimensional system encountered at each time step. Numerical experiments show that using similar space approximations for velocity and density leads to spurious oscillations, which disappear if one employs the same type of elements as those used in the incompressible case for velocity and pressure. Numerical experiments show that the methodology described here provides a good basis for compressible viscous flow calculations. However, there is still room for progress and we are presently working on various improvements concerning the preconditioning, the approximations and the control of oscillations close to sharp layers and shocks.

ACKNOWLEDGEMENT

This work was partly supported by a grant from DRET (Grant No. 88.103), and by NSF (Grant INT 8612680).

REFERENCES

1. M. O. Bristeau, R. Glowinski and J. Périaux, 'Numerical methods for the Navier–Stokes equations. Applications to the simulation of compressible and incompressible viscous flows', *Computer Physics Report 6*, North-Holland, Amsterdam, 1987, pp. 73–187.
2. O. Pironneau and J. Rappaz, 'Numerical analysis for compressible viscous adiabatic stationary flows', in *IMPACT of Computing in Science and Engineering*, Academic Press, Boston, MA, 1989, pp. 1, 109–137.
3. R. Glowinski, *Numerical Methods for Nonlinear Variational Problems*, Springer, New York, 1984.
4. M. O. Bristeau, O. Pironneau, R. Glowinski, J. Périaux, P. Perrier and G. Poirier, 'On the numerical solution of nonlinear problems in fluid dynamics by least squares and finite element methods (II). Application to transonic flows simulations', *Comput. Methods Appl. Mech. Eng.*, **51**, 363–394 (1985).
5. Y. Saad and M. H. Schultz, 'GMRES: a generalized minimal residual algorithm for solving nonsymmetric linear systems', *SIAM J. Sci. Stat. Comput.*, **7**, 856–869 (1986).
6. P. N. Brown and Y. Saad, 'Hybrid Krylov methods for nonlinear systems of equations', *Lawrence Livermore National Laboratory Research Report UCLR-97645*, November 1987.
7. L. B. Wigton, N. J. Yu and D. P. Young, 'GMRES acceleration of computational fluid dynamics codes', *AIAA 7th Computational Fluid Dynamics Conf.*, Cincinnati, OH, July 1985, Paper 85-1494, pp. 67–74.
8. C. Bègue, M. O. Bristeau, R. Glowinski, B. Mantel and J. Périaux, 'Acceleration of the convergence for viscous flow calculations', in C. N. Pande and J. Middleton (eds.), *Numeta 87, Vol. 2*, Martinus Nijhoff, Dordrecht, 1987, pp. T4/1–T4/20.
9. M. Mallet, J. Périaux and B. Stoufflet, 'On fast Euler and Navier–Stokes solvers', *Proc. 7th GAMM Conf. on Numerical Methods in Fluid Mechanics; Notes on Numerical Fluid Mechanics, Vol. 20*, Vieweg, Braunschweig, pp. 199–210.
10. P. N. Brown, 'A local convergence theory for combined inexact-Newton/finite difference projection methods', *SIAM J. Numer. Anal.*, **24**, 407–434 (1987).
11. V. Girault and P. A. Raviart, *Finite Element Methods for Navier–Stokes Equations*, Springer, Berlin, 1986.
12. M. O. Bristeau, R. Glowinski and J. Périaux, 'Acceleration procedures for the numerical simulation of compressible and incompressible viscous flows', in J. S. Doltsinis (ed.), *Advances in Computational Nonlinear Mechanics, CISM Courses No. 300*, Springer, New York, 1989, pp. 197–243.
13. F. Brezzi, 'On the existence, uniqueness and approximation of saddle point problems arising from Lagrangian multiplier', *RAIRO, Sér. Anal. Numér.*, **R2**, 120–151 (1974).
14. D. N. Arnold, F. Brezzi and M. Fortin, 'A stable finite element for the Stokes equations', *Calcolo*, **21**, 337 (1984).
15. M. Fortin and A. Soulaimani, 'Finite element approximation of compressible viscous flows', in H. Niki and M. Kawahara (eds.), *Proc. Computational Methods in Flow Analysis, Vol. 2*, Okayama University of Sciences Press, 1988, pp. 951–956.

16. M. O. Bristeau, R. Glowinski, J. Périaux and H. Viviand (eds.), *Numerical Simulation of Compressible Navier–Stokes Flows, A GAMM Workshop; Notes on Numerical Fluid Dynamics, Vol. 18*, Vieweg, Braunschweig, 1987.
17. B. Palmerio, 'Self adaptive FEM algorithms for the Euler equations', *Rapport de Recherche INRIA Sophia-Antipolis, No. 338*, 1985.
18. C. Pouletty, 'Génération et optimisation de maillages éléments finis. Application à la résolution de quelques équations en mécanique des fluides', *Thèse de Docteur-Ingénieur*, Ecole Centrale, Paris, 1985.
19. M. O. Bristeau and J. Périaux, 'Finite element methods for the calculation of compressible viscous flows using self-adaptive mesh refinements', *Lectures Notes in Computational Fluid Dynamics*, Von Karman Institute for Fluid Dynamics, Rhode-St-Genèse, Belgium, 1986.
20. L. Dutto, *Thesis*, Université Pierre et Marie Curie, Paris (1990).
21. G. Rogé, 'Approximation mixte et acceleration de la convergence pour la résolution des équations de Navier–Stokes compressible en éléments finis', *Thèse de 3ème Cycle*, Université Pierre et Marie Curie, Paris 6, 1990